Robust Solid-Electrolyte Interphase (SEI) formation on Si Anodes Using Glyme-based Electrolytes

Guang Yang*¹, Sarah Frisco², Runming Tao³, Nathan Philip¹, Tyler H. Bennett¹, Caleb Stetson², Ji-Guang Zhang⁴, Sang-Don Han², Glenn Teeter², Steven P. Harvey², Yunya Zhang⁵, Gabriel M. Veith¹, Jagjit Nanda*¹

- 1. Chemical Sciences Division, Oak Ridge National Laboratory, Oak Ridge, TN 37831, United States
- 2. Materials and Chemical Science and Technology Directorate, National Renewable Energy Laboratory, Golden, CO 80401, United States
- 3. Department of Chemistry, the University of Tennessee Knoxville, Knoxville, TN 37996, United States
- 4. Energy Processes & Materials Division, Pacific Northwest National Laboratory, Richland, Washington 99354, United States \$present address: Idaho National Laboratory, Idaho Falls, ID, United States
- 5. Chemical Sciences and Engineering Division, Argonne National Laboratory, Lemont, Illinois 60439, United States

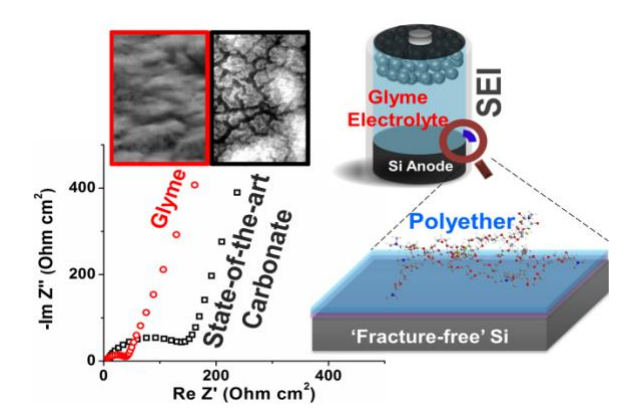
*corresponding authors <u>vangg@ornl.gov</u> <u>nandaj@ornl.gov</u>

This manuscript has been authored by UT-Battelle, LLC under Contract No. DE-AC05-00OR22725 with the U.S. Department of Energy. The United States Government retains and the publisher, by accepting the article for publication, acknowledges that the United States Government retains a non-exclusive, paid-up, irrevocable, worldwide license to publish or reproduce the published form of this manuscript, or allow others to do so, for United States Government purposes. The Department of Energy will provide public access to these results of federally sponsored research in accordance with the DOE Public Access Plan (http://energy.gov/downloads/doe-publicaccess-plan).

Abstract

Silicon (Si) is the most naturally abundant element possessing 10-fold theoretical capacity than graphite-based anodes. The practicality of implementing Si anodes is, however limited by the unstable solid-electrolyte interphase (SEI) and anode fracturing during continuous lithiation/delithiation. We demonstrate that glyme-based electrolytes (GlyEls) assure a conformal SEI on Si and keep the Si 'fracture-free'. Benchmarking against the optimal, commonly-used carbonate electrolyte with the fluoroethylene carbonate (FEC) additive, Si anode cycled in a GlyEl exhibits reduced early parasitic current (by 62.5%) and interfacial resistance (by 72.8%), while the cell capacity retention is promoted by >7% over a course of 110 cycles. The mechanistic investigation by X-ray photoelectron spectroscopy (XPS) and energy-dispersive X-ray spectroscopy (EDX) indicates GlyEl enriches Si SEI with elastic polyether but diminishes its carbonate species. Glyme-based electrolytes prove viable in stabilizing the SEI on silicon for future high energy density lithium-ion batteries.

TOC GRAPHICS



Due to its ultrahigh theoretical lithium storage capacity (3579 mAh g⁻¹ for Li₁₅Si₄), ¹ silicon has been considered as a promising alternative anode to graphite in lithium-ion batteries (LIBs). ²⁻³ Electrolytes are one of the most essential components and are often determinative in the cycling stability of LIBs. ⁴ The reduction decomposition of the electrolyte components generates a passivation layer, the so-called solid/electrolyte interphase (SEI), to protect the electrolyte from further decomposition. ⁵ Common carbonate-based electrolytes (CarEls) optimized to stabilize the graphite anode/electrolyte interphase for state-of-the-art LIBs ⁶ insufficiently passivate the silicon anode. ⁷ Structural disruption during cycling results in ~300% volumetric change of the Si anode. ⁸ The subsequent Si fracture inevitably deteriorates the superficial SEI layer. Further, the decomposition products of the CarEls such as lithium ethylene dicarbonate (LiEDC) are reactive on Si surface. ⁷ Taken together, the application of CarEls generates an inherently unstable SEI, leading to continuous electrolyte decomposition and Li consumption on Si surface, causing rapid degradation of the LIB over time.

Extensive attempts have been made to promote Si cyclability using carbonate-based additives. ⁹⁻¹⁰ An addition of less than 10 wt% fluoroethylene carbonate FEC has been shown to drastically improve the charge/discharge stability. ¹¹⁻¹² The beneficial role of FEC degradation in stabilizing Si anodes is thought to occur via a) facilitating earlier formation of the passivation layer at a higher reduction potential to mitigate the decomposition of other electrolyte components, and ¹² b) mitigating the poly(ethylene oxide) (PEO)-like oligomeric electrolyte breakdown products by forming a cross-linked polyether network. ¹³ The insolubility of the cross-linked polymeric species appears crucial to accommodating severe Si volumetric change upon cycling, thereby stabilizing the Si surface and enabling capacity retention. ¹³⁻¹⁴ Despite early successes, carbonate additives have seen intrinsic limitations to ameliorate instability of the SEI on Si.

Glyme-based electrolytes (GlyEls) have proved beneficial in stabilizing lithium metal anodes. ¹⁵ In the presence of concentrated electrolytes, GlyEls are capable of suppressing lithium dendrite growth. ^{4, 16} Early efforts in GlyEl development were primarily focused on improving cyclability of silicon sulfur batteries. ¹⁷⁻¹⁹ 1,3-dioxolane (DOL) in dimethoxyethane (DME) solvents were often used, with lithium nitrate (LiNO₃) additive to mitigate the polysulfide shuttle effect. ¹⁷ To date, investigation of GlyEls as an electrolyte chemistry to stabilize Si anodes has been unexplored. As a result, knowledge of the SEI chemistry, structure, and formation mechanism in GlyEls on Si is largely absent.

In this work, we demonstrate that GlyEls outperform their carbonate-based analogues by forming a more robust SEI on Si. Lithium bis(fluorosulfonyl)imide (LiFSI) in DME was used as a model GlyEl, with or without the 1,1,2,2-tetrafluoroethyl-2,2,3,3-tetrafluoropropyl ether (TTE) additive. TTE is analogous to the FEC additive for carbonates. GenII (1.2M LiPF₆ in ethylene carbonate (EC):ethyl methyl carbonate (EMC), 3:7 wt.%) was used as the GlyEl counterpart. The addition of 10 wt% FEC to GenII leads to an optimal CarEl (GenF) with improved cycling performance. Comparison of initial and long-term cycling SEI on a 50 nm amorphous silicon (a-Si) thin film anode in a Li-Si half-cell were performed between GlyEls and CarEls. A GlyEl composed of LiFSI, DME and TTE (1:3:3 by molar ratio, denoted as LiFSI-3DME-3TTE, corresponding to 1.2M LiFSI in DME assuming TTE does not participate in the coordination chemistry) surpassed its best performing CarEl counterpart, GenF, with enhanced cycling performance, reduced interfacial resistance and polarization effect. LiFSI-3DME-3TTE was found capable of stabilizing Li metal anode.²⁰ Its functions on Si anode have yet been explored. Structural and morphological investigation indicates that SEI formed with LiFSI-3DME-3TTE is more conformal on Si after prolonged cycles, protecting Si from fracturing. Chemical characterization indicates that such a SEI has reduced carbonate but increased polyether compounds compared to its carbonate counterparts, providing a more elastic and Li⁺-conductive SEI on Si anode.

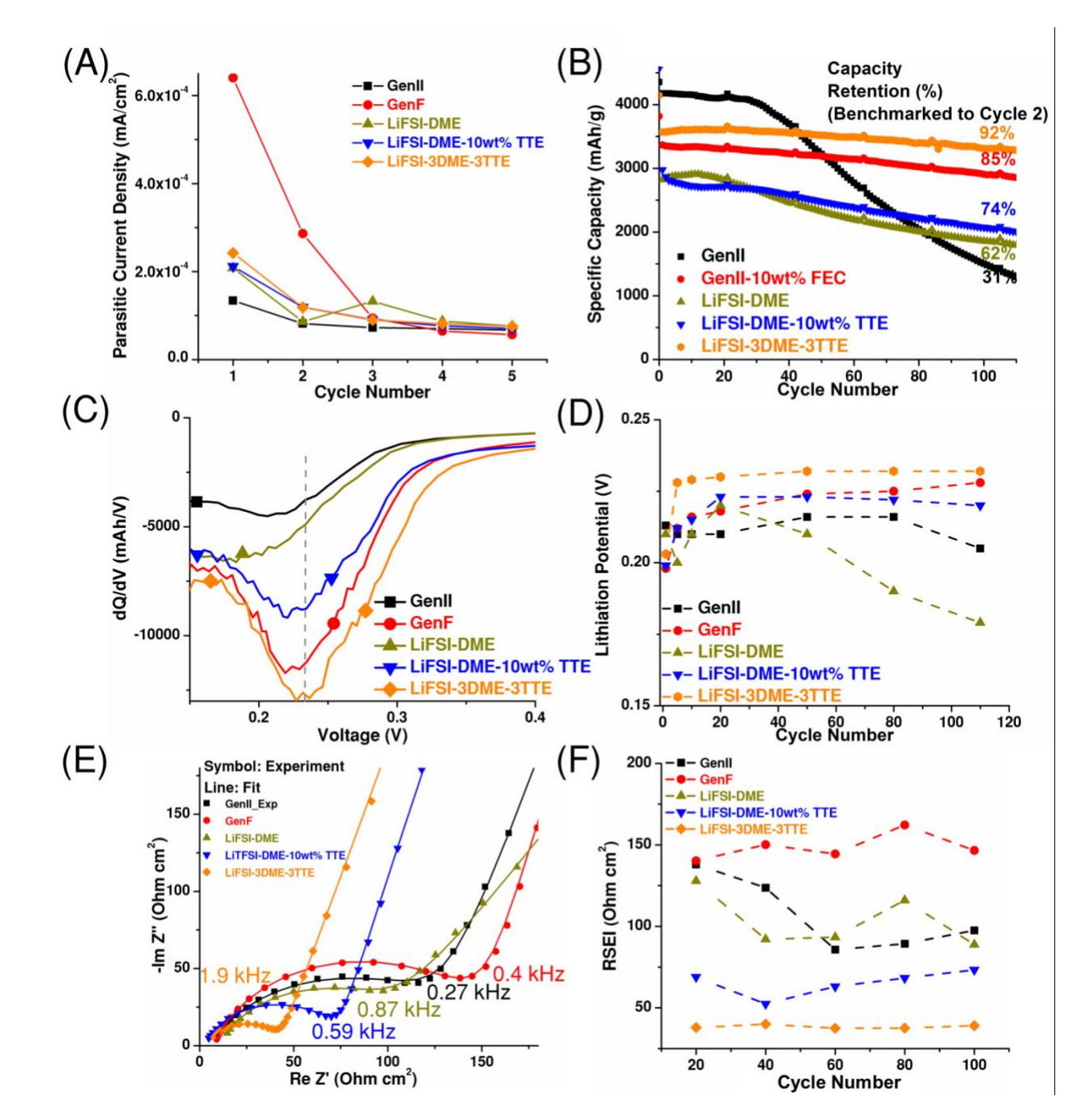


Figure 1. (A) Summary of the parasitic current density collected at the end of the 24h chronoamperometry holding test. All galvanic cycling was implemented at 1C equivalent rate (41.7 μ A/cm²) between 50 mV and 1.5V at 25° C. (See Fig S1.E-F for test protocol) (B) Discharge capacity as a function of cycle number. (C) Comparison of the lithiation peaks for various electrolytes (see Fig S2 for dQ/dV plot overview). (D) The lithiation potential as a function of cycle number for a-Si anodes cycled in various electrolytes. (E) EIS plots for various electrolytes at the 100th cycle. The frequency value was taken from the semi-circle top for each sample. (F) Values of SEI resistance, R_{SEI} , for various electrolytes at different cycling stages (See Figure S4 for EIS overview).

Early SEI formation was first studied by cyclic voltammograms (CVs) as summarized in Fig S1.A-D. GenII electrolyte features a reduction potential at 0.76 V (vs. Li/Li⁺, hereafter), indicating the EC onset reduction (Fig S1.B). ²¹ GenF has an elevated SEI formation voltage at 0.79V, related to the sacrificial FEC decomposition, which mitigates the decomposition of other electrolyte components. ²²⁻²³ All GlyEls exhibit an initiation of reduction at higher potentials than CarEls. GlyEls with TTE have noticeably increased cathodic current (Fig S1.B), indicating that TTE may serve as a protective agent or promote the protective electrolyte reduction analogous to FEC in GlyEls.

Under optimal conditions, the Si anode should be well passivated during early cycling to mitigate excess electrolyte decomposition. To investigate the initial passivation period, the SEI formation behavior on a-Si in early galvanostatic cycles was first explored. Galvanostatic cycling (GC) – chronoamperometry (CA) holding protocol was used to complement initial SEI stability on a-Si (Fig S1.E-F). Briefly, the a-Si thin film anodes were pre-cycled in the different electrolytes at 1C rate (i.e. formation cycle) between 50 mV and 1.5 V and 50 mV, followed by five discharge (at 1C rate to 50 mV) – CA hold (at 50 mV for 24h)-charge (at 1C rate to 1.5V)-cycles as shown in Fig S1.E-F. It is assumed that there is no net change of the alkali ions in the anode at the end of the CA holding stage, with the ending stage current defined as the parasitic current, I_p . I_p quantifies the continuous electrolyte decomposition on lithiated Si surface due to incomplete SEI coverage. GenII exhibits the lowest I_p in the first GC, whereas GenF has 4.8-fold larger I_p , indicating more electrolyte was consumed in GenF for a-Si surface passivation (Figure 1A).

GlyEls show an intermediate I_p values in the 1^{st} cycle compared to those of CarEls. Without TTE, the parasitic current fluctuates over cycling, likely due to incremental dissolution of the SEI layer over time. Therefore, TTE is necessary to stabilize Si anode for GlyEls. Overall, I_p deceases nearly exponentially over cycling, indicative of progressive SEI passivation of a-Si with all electrolytes. The evaluation of early passivation behavior on Si indicates that even with the optimal additive, FEC, the SEI formed on Si is unstable in early GC cycles. The GlyEls (with TTE) have marginally larger parasitic current than GenII, but smaller I_p than GenF. This result motivates an exploration of SEI formation after extended cycling to better evaluate the SEIs formed in GlyEls and CarEls.

When cycled with LiFSI-3DME-3TTE, a-Si exhibits more stable charge-discharge profiles (Fig S2) and the smallest initial capacity loss (Fig S2.A and Table S1). Another primary advantage of LiFSI-3DME-3TTE over other electrolytes is its promoted capacity and capacity retention. Adding 10 wt% TTE increases the capacity retention from 62% to 74% compared to LiFSI-DME, showing the importance of TTE as an additive in GlyEls. All GlyEls measure higher capacity retention than GenII. Notably, the average capacity of LiFSI-3DME-3TTE is 12.3% higher than GenF, with capacity retention over 7% higher than GenF. The discharge capacity was 3266 mAh/g for LiFSI-3DME-3TTE at 110th cycle, 15% larger than GenF. It should be noted that higher than theoretical capacity of the Si anode during the initial cycle has been observed for all electrolytes in Figure 1(B), agreeing with similar studies on Si thin film anodes. ²⁴⁻²⁶ The initial capacity reduction of GenII is 96.3%. Both GenF and the LiFSI-3DME-3TTE exhibit higher initial capacity reduction values of 88.7% and 86.2%, respectively. The higher than expected initial capacity and the initial capacity reduction of the thin film a-Si anodes can be ascribed to the both of the SEI formation ²⁵ and the reaction of the Li⁺ with the surface Si_xO or silanol groups. ²⁶ The existence of the Si_xO and silanol groups on the a-Si thin film was confirmed by our recent study. ²⁷ The side reactions between Li⁺ and Si_xO and Si-OH lead to irreversible Li₂O and LiOH formation. ²⁶ Note that the SEI formation may limit the generation of the Li₂O and LiOH, the different initial capacity reduction values among various electrolytes is likely due to the different initial SEI layers produced in various electrolytes and the consequent different amount of Li₂O and LiOH formation.

In addition to improved capacity and capacity retention compared to GenF, LiFSI-3DME-3TTE shows stable Columbic efficiency (CE) at an earlier point in cycling (>99%, 4th cycle (Fig S3)). In contrast, GenF did not reach 99% CE until the 6th cycle. GlyEls without TTE did not achieve 99% CE until 60 cycles, supporting the importance of TTE additive in the suppression of side reactions which occur earlier than those associated with FEC additive in GlyEl. Interestingly, both LiFSI-DME-10wt% and GenII show CE <98.5%, with the maximum CE values in the 16th cycle, indicating the importance of sacrificial additives such as TTE and FEC in the stabilization of Si anodes. LiFSI-3DME-3TTE enables an average CE of 99.4% in the final 30 cycles, comparable to state-of-the-art carbonate electrolytes ³ and artificial SEIs engineered for the a-Si thin film anode. ²⁸⁻²⁹

LiFSI-3DME-3TTE also demonstrates the lowest polarization, facilitating lower energy barriers to lithiation and delithiation. Differential capacity profiles (Fig S2.A) show two lithiation peaks at 0.07V and 0.20V (Figure 1(C)) after the 1st cycle, and two delithiation peaks at 0.30V and 0.49V. The lithiation potentials for LiFSI-3DME-3TTE are high in the first 5 cycles (Figure 1(D) and Fig S2), demonstrating its low energy barrier for Si lithiation. Si anode passivation results in increase of the polarization effect upon cycling. ³⁰ Counter-intuitively, polarization decreases for all electrolytes after the 1st charge/discharge cycle, despite additional SEI growth. Electrochemical impedance spectroscopy (EIS) profiles (Fig S4) show an abrupt drop in anode/electrolyte interfacial resistance after the 1st cycle, coincident with the decreased polarization depicted in Figure 1(D). Such a phenomenon is likely due to the disruption of the resistive native SiO_x layer on a-Si upon lithiation. ^{26, 31} Notably, polarization decreases for both of LiFSI-3DME-3TTE and GenF upon cycling, whereas other electrolytes show fluctuating lithiation potentials, indicating multiple competing mechanisms in the SEI (Figure 1(D)). Given that continuous lithiation/delithiation leads to expansion/contraction of the Si, the already-formed SEI could be destroyed and Si surface area could be increased due to Si fracture. 32-33 The increased surface area results in an overall reduced anode/electrolyte interfacial resistance in successive cycles. It is noteworthy that the polarization for LiFSI-3DME-3TTE reaches steady-state earlier than GenF, suggesting that a more protective SEI forms more rapidly, agreeing with the smaller parasitic current observed for LiFSI-3DME-3TTE compared to GenF (Figure 1(A)). We shall point out that a small parasitic current at the early galvanostatic cycling stage does not seem to directly correlate to the longterm cycling stability. The possible reason is that more reduction decomposition of the electrolyte is necessary to build the SEI robust to endure volumetric change of the Si. Therefore, future design of Si anode should consider such an effect to compensate the lithium loss during the SEI formation stage.

EIS plots also reveal that a-Si has the lowest interfacial resistance at prolonged cycles in LiFSI-3DME-3TTE (Figure 1(E-F)). A typical EIS curve is composed of a semicircle at medium to high frequency (1MHz – 50Hz) and a low frequency (<50 Hz) diffusion tail (Figure 1(E) and Fig S4). This type of EIS is best described by an equivalent circuit of 6 elements: $R_{electrolyte}+[Q_{SEI}/R_{SEI}]+[Q_{SE}/(R_{SE}+W_d)]$, where the high frequency intercept on the real impedance axis, $R_{electrolyte}$ represents the electrolyte Ohmic loss; the parallel RC circuit, Q_{SEI}/R_{SEI} , represents the resistance from the charge transport across the SEI on a-Si, resistance from charge transport in the SEI, and an additional RC circuit indicates the surface electron transfer process (Q_{SE} and R_{SE}). The Warburg circuit element, W_d models the lithium diffusion resistance in bulk a-Si anode and Q is the constant phase element, representative of nearly capacitive impedance components in the circuit. 34 The experimental and fitted EIS spectra are in good agreement with the suggested equivalent circuit, averaging less than 1.5% deviation as calculated by weighted sum of squares (Figure 1(E)). A plot of the R_{SEI} vs. cycle number is shown in Figure 1(F). While the value of R_{SEI} for LiFSI-3DME-3TTE stabilizes at $38.3\pm0.9~\Omega/cm^2$ after the 20^{th} cycle, R_{SEI} of other electrolytes fluctuates as cycling proceeds, suggesting a lack of passivation layer on a-Si. Notably, the overall interfacial

resistance of LiFSI-3DME-3TTE electrolyte is one quarter that of its GenF counterpart. These results indicate prospective benefits for improved rate performance for Si anodes with glyme electrolytes.

To evaluate the performance of the GlyEls with more practical electrodes, a proof-of-concept full cell test using the particle-based composite Si anode and a high voltage LiNi_{0.5}Mn_{0.3}Co_{0.2}O₂ (NMC532) cathode was performed. As shown in Fig S5, the charge/discharge galvanostatic cycling curve looks similar for LiFSI-3DME-3TTE benchmarked to GenF. Overall, cycled with LiFSI-3DME-3TTE electrolyte, the Si-NMC(532) full cell shows marginally higher discharge capacity in 20 cycles. It indicates that the GlyEls is potentially compatible with high voltage cathodes.

Salt concentration effect on the parasitic current and the cycling performance of the a-Si thin film anode was also investigated as shown in Fig S6. With saturated LiFSI in DME (LiFSI-1.2DME-3TTE, corresponding to 3M LiFSI in DME), the parasitic current was further reduced during the first 5 cycles. However, the specific capacity was reduced benchmarked to LiFSI-3DME-3TTE, likely due to the increased ion cluster concentration in the GlyEl and reduced ionic conductivity (see Supporting Information for details)

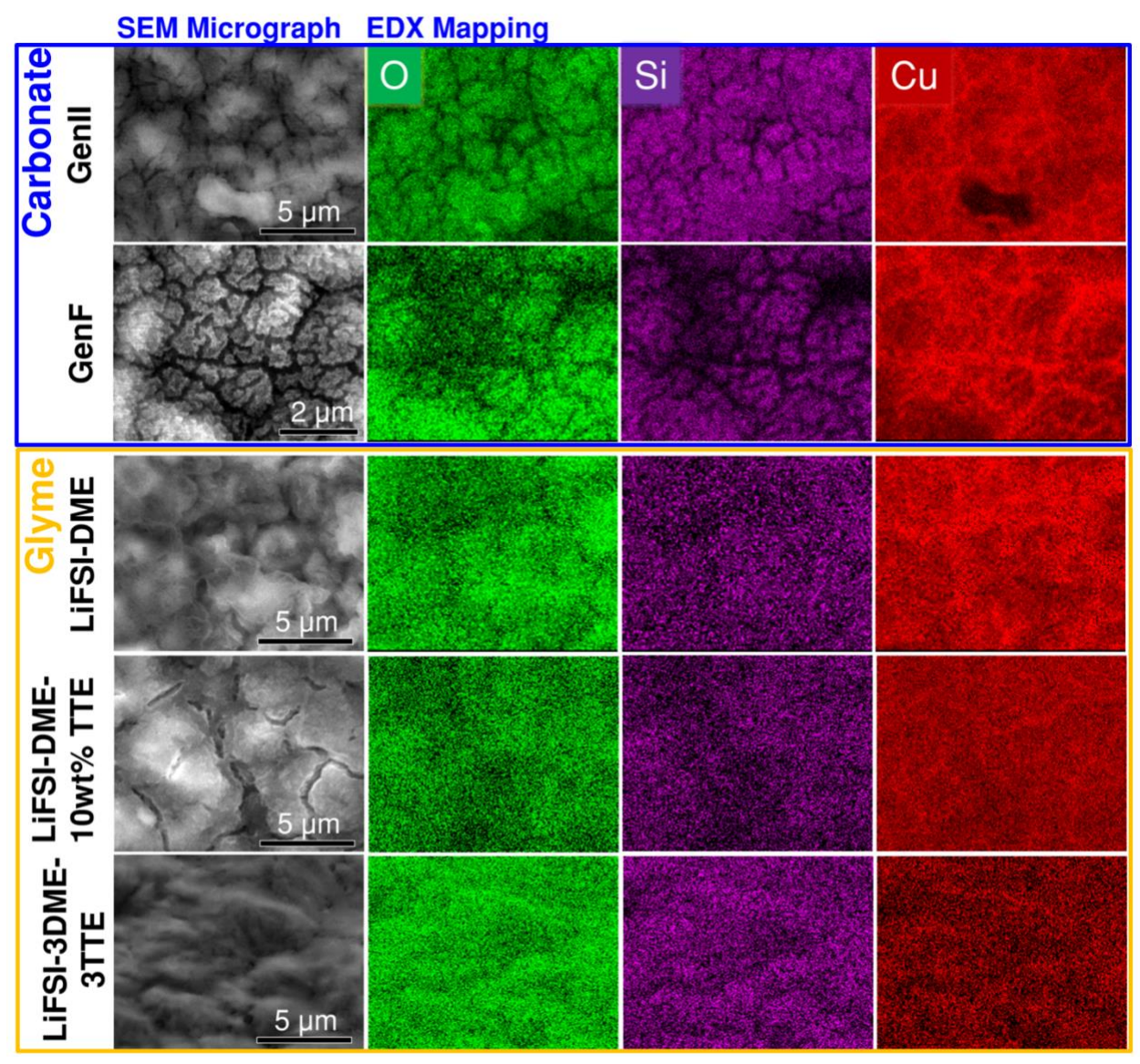


Figure 2. SEM micrographs and corresponding SEM-EDX maps of a-Si anodes after 110 cycles in various electrolytes. The oxygen and silicon mappings represent the SEI and Si distribution on Cu foil, respectively. Cu maps are complementary to Si maps, where underlying Cu is exposed in fractured regions of the Si. The SEM image of the pristine Si is shown in Fig S7.

Further investigation of the a-Si anode morphology and chemistry via scanning electron microscopy (SEM) and energy-dispersive X-ray spectroscopy (EDX) mapping shows that LiFSI-3DME-3TTE facilitates the formation of a "crack-free" a-Si anode and a conformal SEI coating. As manifest in the SEM micrographs, small fractures develop in the a-Si cycled in CarEls (see Fig S5 for pristine a-Si SEM); in contrast, fewer cracks form on a-Si cycled in GlyEls. Particularly, a-Si cycled in LiFSI-3DME-3TTE shows minimal fracture. Particularly, a-Si cycled in LiFSI-3DME-3TTE shows minimal fracture. The a-Si fracture may initiate in the preliminary five cycles (see Fig S8). The presence of higher spectroscopic intensity for Cu at sites of low Si intensity confirms the occurrence of the morphologically evident Si fracture. From these observations of Si fracture, the CarEl SEI (CarEl-SEI) appears incapable of uniform passivation, as indicated by the inhomogeneity in the O signal. In contrast, LiFSI-3DME-3TTE aids in forming a uniform and conformal SEI, as evidenced by the homogenous O signal. Without TTE, the SEI

occurs in an island-like pattern, with visible a-Si fracture. LiFSI-3DME-3TTE promotes the integrity of the Si and SEI through 110 cycles, benefiting the improved capacity and capacity retention. It should be noted that the existence of the Si-oxide components also contributes to the oxygen signal. However, such a contribution is considered small (<5%), with further evidence from the XPS detailed in the supporting information.

EDX atom% analysis (Fig S9) suggests that LiFSI-3DME-3TTE has the highest carbon (68.6 C atom%) among all electrolytes, indicating that LiFSI-3DME-3TTE promotes the polymeric-rich SEI composition (i.e. C-C backbone). After 110 cycles, GlyEl-SEI has nearly three times higher F content than the CarEl-SEI counterparts, independent of TTE loading (Fig S9). This result suggests that LiFSI decomposition is a major source of fluorinated species in GlyEl-SEI.

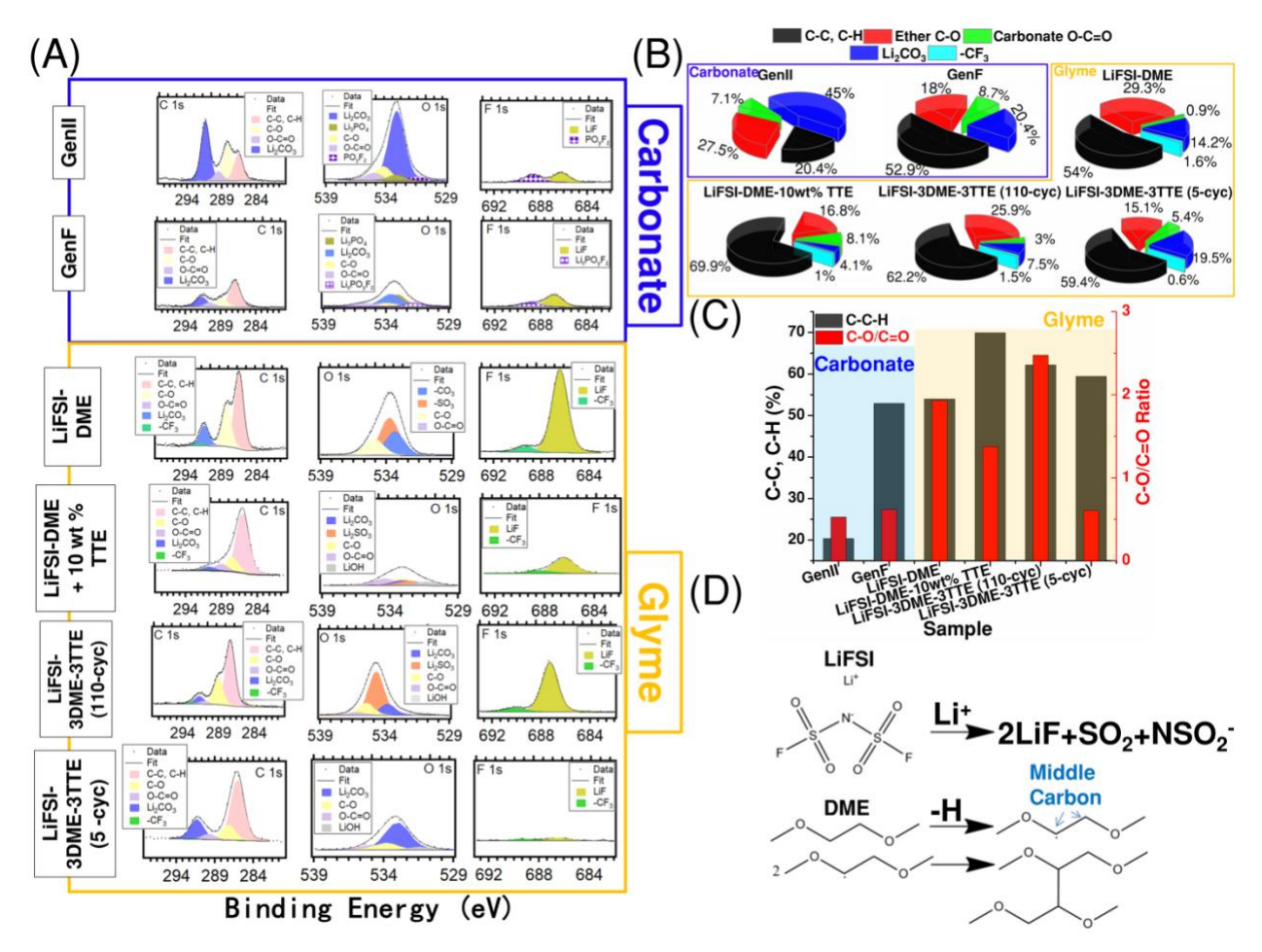


Figure 3. (A) XPS C 1s, O 1s and F 1s core-levels of a-Si cycled in different electrolytes after 110 cycles (110-cyc) and only in LiFSI-3DME-3TTE after 5 cycles (5-cyc). (B) C% atom ratio for different functional groups on a-Si for various electrolytes. (C) Comparison of aliphatic (C-C, C-H) atomic percentages and relative ratios of C-O/C=O for different Si SEIs. (D) Decomposition mechanisms of LiFSI and DME in GlyEls.

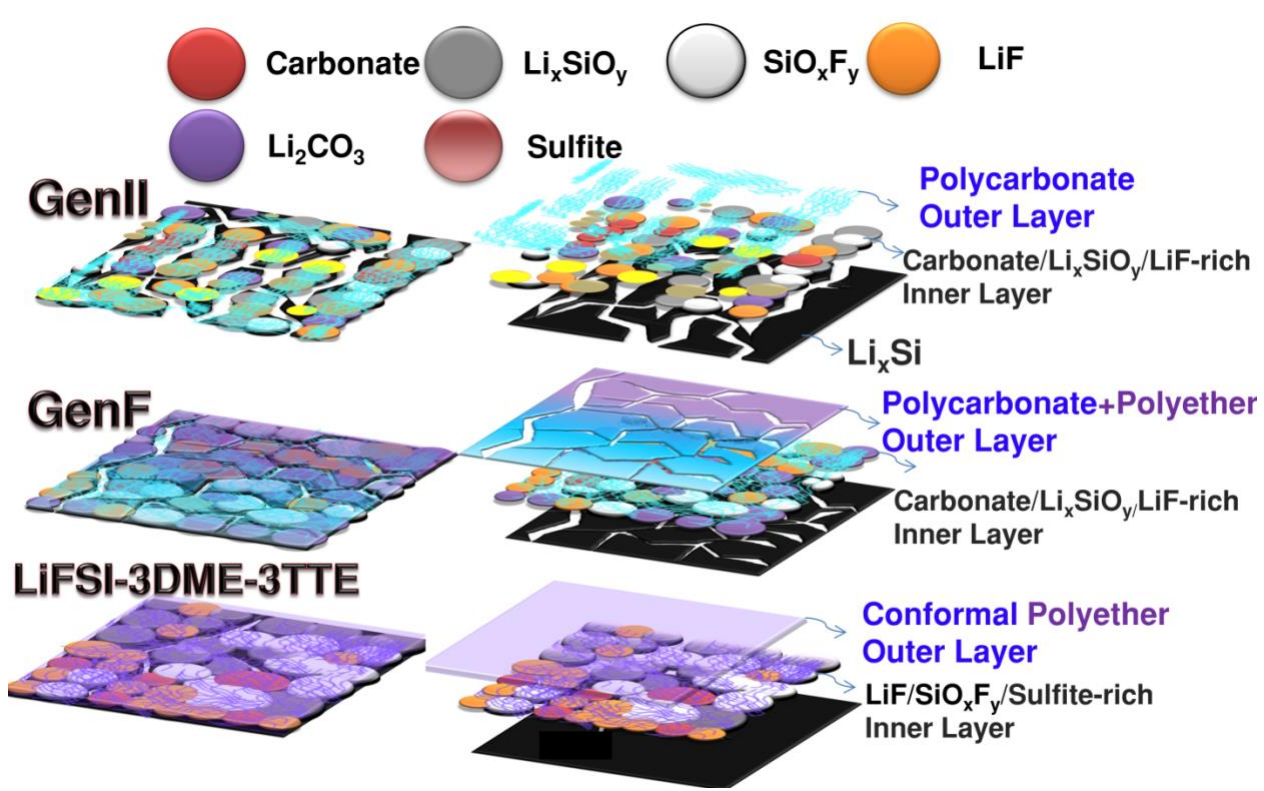
X-ray photoelectron spectroscopy (XPS) was used to explore the compositional differences between the SEI of each electrolyte. Fig S10 shows that the SEI in all electrolytes contains high concentrations of C, O and Li, and low concentrations of F and Si. Focusing on C 1s core-level, the most distinct chemical difference between the CarEl-SEI and the GlyEl-SEI lies in the peak at

290.7-291.7 eV. This peak represents the carbonate compounds (Table S2). 35-36 Such a peak has noticeably larger intensity in GenII SEI after 110-cycle compared to the same peak in the GlyEl-SEI. The second noticeable difference between GlyEl-SEI and CarEl-SEI is that the former contains larger concentration of ether (C-O) groups, as manifested by the higher intensity of the 287.2-289.8 eV C 1s peak. ³⁷ The relative prevalence of carbonyl in the CarEl-SEI and ether in the GlyEl-SEI is also observed in the O 1s spectra shown in Figure 3. Interestingly, the carbonate peak is significantly more dominant for the first 5 cycles of the LiFSI-3DME-3TTE, but then is shown to be severally diminished by the 110th cycle. A more quantitative analysis on XPS C1s peak is detailed in Figure 3(B). As reported by Grey et al., 13 FEC facilitates the formation of cross-linked PEO stemming from multi-electron reduction of EC. The elasticity of the PEO species aids in buffering the volumetric change of Si. 13 For clarification, the "elasticity" here is to describe the mechanical property of the polymeric SEI layer, which scales the SEI reversible deformation to endure the stress variation in repetitive lithium insertion and extraction process in the Si anode. Other studies also found the permanent plastic deformation of the Si is more important than the elasticity. ³⁸⁻³⁹ The GlyEl-SEI formed in LiFSI-3DME-3TTE has 1.3× larger ether concentration than its CarEl-SEI counterpart from GenF. Its alkyl C-C/C-H (286-287.34 eV) ⁴⁰ is 1.2× of the GenF CarEl-SEI. This clearly indicates that SEI derived from LiFSI-3DME-3TTE is enriched in polyether (i.e. PEO). This finding can be further consolidated by C-O/C=O and carbon/oxygen (C/O) ratios. Figure 3(C) clearly shows that the C-O/C=O ratio is higher for GlyEl-SEI than its ClyEI counterpart. C/O ratio serves as a side-proof of the relative abundance of the carbonate and ether based on the following reason. The C/O ratios are 2, 0.5 and 0.33 for single ethylene oxide unit (-C-C-O), carboxylate group (-COO), and carbonate (OC=OO), respectively. It can be clearly seen from Fig S11 that GlyEl-SEIs have an overall higher C/O ratio than their CarEl-SEI counterparts after 110-cycle. Compared to the GenF CarEl-SEI, the LiFSI-3DME-3TTE (110-cycle) GlyEl-SEI has a greater than 3× C-O/C=O ratio and greater than 2× C/O ratio, suggesting a much higher polyether abundance in GlyEl-SEI. We herein propose a possible cross-linking decomposition mechanism of DME illustrated in Figure 3(D). An ethane group in the middle may lose hydrogen to form a DME-radical. 41 Crosslinking reactions could then occur among the DME· radicals to form a polyether network. As previously mentioned, early SEI formed in LiFSI-3DME-3TTE (5-cycl) has $2.6\times$ more carbonate compounds, but $1.7\times$ less ether concentration than its 110-cycle counterpart. Having a lower polyether concentration at early cycles may contribute to a less stable SEI (Figure 1). The enrichment of polyether after prolonged cycles of GlyEl-SEI has four potential merits: (i) it reduces solvent penetration and swelling of the SEI helping to mitigate further solvent reduction; (ii) it has higher elasticity compared to the polycarbonate counterpart, thereby mitigating the cracking in the SEI and accommodating the Si volumetric change and (iii) it promotes higher Li⁺ conductivity than linear PEO from EC-based CarEls; 42 (iv) the conformal SEI coating may homogenize the Li⁺ transport through the SEI, thereby synchronizing the volumetric change of Si from point to point and mitigate the Si fracturing overtime. ⁹

A higher polyether concentration is not a guaranteed sign of a "better" SEI and more stable cycling. All GlyEl-SEIs have a higher polyether loading than GenF CarEl-SEI; however, Li-Si cells with LiFSI-DME and LiFSI-DME-10wt% TTE showed worse cycling performance than GenF (Figure 1(B)). Figure 3(B) shows that GlyEl-SEI formed in LiFSI-DME contains twice the amount of Li₂CO₃ (290.7-291.7 eV) ⁴⁰ as GlyEl-SEI formed in LiFSI-3DME-3TTE. This increased presence of Li₂CO₃ hinders Li⁺ transport due to its low Li⁺ conductivity. Therefore, it is critical to consider Li⁺ conductivity in addition to the SEI elasticity. ⁴³

Fluorinated species have a significant impact on how the SEI behaves during cycling. From Figure 3(A), F 1s core-level spectra show that the all GlyEl SEIs have increased LiF (686.2-687.2 eV) concentration

compared to CarEl SEIs. Studies have yet to reach a consensus on the function of LiF in the SEI. ⁴⁴⁻⁴⁵ On the one hand, LiF formation in the SEI layer is essential to create an electron barrier to keep the electrolyte from further degradation. ⁴⁶ On the other hand, a high LiF concentration in the SEI could block electron transfer, thereby increasing the internal resistance of the Li-Si cell and ultimately reducing the cell cycle life. ⁴⁴ Without the TTE additive, GlyEl SEI formed in LiFSI-DME has 1.3× more LiF than its LiFSI-3DME-3TTE counterpart (Fig S12), whereas the addition of 10wt% TTE leads to 40% less LiF. It indicates that the amount of LiF needs to be optimized for a better performing SEI. The abundance of fluorinated species in all GlyEl-SEI samples is independent of the TTE loading, suggesting that the fluorinated species result preferably from the decomposition of LiFSI instead of TTE. This agrees with the EDX analysis. A possible LiFSI decomposition path is shown in Figure 3(D). A multiple electron transfer to LiFSI leads to cleavage of the S-F bond, and consequent formation of N(SO₂)₂ species. ⁴¹ Further decomposition of N(SO₂)₂ leads to SO₂ gassing, or formation of the SO₃²⁻ in GlyEl-SEIs (also see Fig S13). ⁴⁷ There is no SO₃²⁻ in the CarEl-SEIs. Sulfite containing SEI was found capable of stabilizing graphitic anodes, ⁴⁸ but whether or not it can stabilize Si anodes is not yet clear and should be subject to further exploration.



Scheme I. Illustrations of the composite (left) and partitioned (right) views of the SEIs formed in CarEls and GlyEl after extended cycling. GlyEl-SEI formed in LiFSI-3DME-3TTE is more conformal to reduce Si anode fracture, with different SEI inner and outer layer components compared to CarEl-SEIs.

We further explore the synergy of the SEI formation and the Si fracture for different electrolytes. It should be noted that the lithiation/delithiation induced fracturing on an amorphous silicon thin film anode is different than that observed in a polycrystalline silicon particle due to smaller in-plane strains on the thin film Si anode. ³⁸ Xia and coauthors showed that a critical film thickness of the Si thin film on copper substrate was estimated to be 100–200 nm, below which the tensile stress zone diminishes and fracture would be mitigated. ⁴⁹ The a-Si thin film used in the current study has a thickness of 50 nm, lower than the critical value where fracture could be observed. However, the a-Si thin film anodes cycled in

carbonate based electrolytes at 1C rate and in LiFSI-3DME-3TTE at 2C rate clearly show Si fracturing after 110 cycles. Cheng and Verbrugge pointed out that the Li⁺ diffusion plays an essential role in crack initiation and formation on Si anodes. ⁵⁰ Based on the insights of abovementioned studies and what has been observed (Figure 2 and Fig S8), we propose the following Si fracturing mechanism observed in the current study.

The use of LiFSI-3DME-3TTE could not perfectly avoid Si fracturing, as evidenced by Fig S8 where cracks were observed for a-Si anode in early cycles, with smaller number of cracks benchmarked to the carbonate electrolytes. This may be explained by that the fluorine-rich inner SEI layer generated in LiFSI-3DME-3TTE provides higher elastic moduli, ^{39, 51} assisting in the fracture mitigation at an early galvanostatic cycling stage. At this stage, the organic SEI layer has not been sufficiently developed as island SEI structure could be observed on the a-Si surface (Fig S8 bottom). As cycling prolongs, a more conformal organic SEI layer rich in PEO forms on the a-Si. The existence of such a conformal outer SEI layer facilities the homogeneous ion transport on a-Si surface, thereby mitigating the Si fracturing. Notably, the layered SEI structure has been reported on a similar study. ³⁹ In construct, due to the inhomogeneous SEI formation in carbonate electrolyte, Li⁺ transport on the anode surface turns to be heterogeneous, thereby leading to the heterogeneous lithiation of the a-Si and diffusion-induced stress on the a-Si and the consequent Si fracturing. Such a statement is further evidenced by the C-rate effect shown in Fig S14. At the 2C rate, LiFSI-3DME-3TTE electrolyte is no longer capable of keeping the a-Si "crack-free". This issue may be ascribed to the uneven current distribution and the consequent heterogeneous Li⁺ ion insertion to the a-Si anode, which is known to cause the uneven stress distribution in Si upon lithiation. ⁵⁰ (See Supporting Information for the detailed discussion) Therefore, prevalent cracks can be observed for a-Si cycled in LiFSI-3DME-3TTE. It is thus advisable to explore the structure and conformability of the SEI and Si fracturing synergistically.

In conclusion, this work demonstrates that the glyme-based electrolytes are promising to form a robust SEI layer on Si anode. More specifically, SEI formed on Si anode with LiFSI-3DME-3TTE, outperforms the SEI of its best carbonate electrolyte counterpart, GenF. The GlyEl-SEI exhibits a more conformal coating on Si, mitigating the fracture formation on Si anodes after extended cycling. The chemical structure of this GlyEl-SEI is intrinsically different from the SEIs formed in traditional carbonate-based electrolytes, as summarized in Scheme I. The enriched polyether in the outer GlyEl-SEI is elastic to endure the stress variation in repetitive lithium insertion and extraction process in the Si anode, thereby enabling a conformal SEI on Si. Such a conformal SEI layer benefits homogenous a homogenous lithiation/delithiation of Si, further alleviating a-Si thin film fracture. The inner GlyEl-SEI layer features a reduced amount of carbonate and silicide, and increased LiF, sulfite and SiO_xF_y. Such a beneficial SEI structure facilitates the improvement of the cell cycling performance and reducing the cell internal resistance and polarization. Although glyme has potential electrochemical stability issues vs. high voltage cathodes, modified glyme electrolytes using dual salts ⁵² or high concentrated electrolytes ²⁰ have shown promising to address such issues. The findings in the current study identify promising alternative electrolyte chemistries for improved interfacial stabilization for next-generation high energy-density Sibased LIBs.

Supporting Information

The Supporting Information is available free of charge on the ACS Publications website at DOI: XXXX Detailed experimental methodologies; CV profiles and galvanostatic cycling (GC) – chronoamperometry (CA) holding protocol for various electrolytes; Coulombic efficiency (CE) evaluation; charge/discharge and differential capacity plots; overview of EIS plots of a-Si in various electrolytes; proof-of-concept full cell test using a Si particle anode and a LiNi_{0.5}Mn_{0.3}Co_{0.2}O₂ (NMC532) cathode; salt concentration effect; SEM micrographs of the pristine a-Si on copper; SEM micrographs and the EDX mapping of a-Si anodes

after 5-cycle; atomic concentration analysis based on XPS spectra; XPS core-level assignment; C-rate effect

Author Information

Corresponding Authors

*Email: yangg@ornl.gov; website: https://www.ornl.gov/staff-profile/jagjit-nanda *Email:nandaj@ornl.gov; website: https://www.ornl.gov/staff-profile/guang-yang

ORCID

Guang Yang: 0000-0003-0583-6272 Steven P. Harvey: 0000-0001-6120-7062 Jagjit Nanda: 0000-0002-6875-0057

Notes

The authors declare no competing financial interest.

Acknowledgement

This work is supported by the US Department of Energy (DOE) Vehicle Technologies Office under the Silicon Electrolyte Interface Stabilization (SEISta) Consortium directed by Brian Cunningham and managed by Anthony Burrell. This manuscript has been authored by UT-Battelle LLC under Contract DE-AC05-00OR22725 with DOE. The electrodes in this article were fabricated at Argonne's Cell Analysis, Modeling and Prototyping (CAMP) Facility. Authors thank Drs. Sheng Dai, Andrew Jansen, Bryant Polzin, and Fulya Dogan Key for experiment support. The US government retains and the publisher, by accepting the article for publication, acknowledges that the US government retains a nonexclusive, paid-up, irrevocable, worldwide license to publish or reproduce the published form of this manuscript, or allow other to do so, for US government purposes. DOE will provide public access to these results of federally sponsored research in accordance with the DOE Public Access Plan (http://energy.gov/downloads/doe-public-access-plan).

Reference

- 1. Obrovac, M.; Christensen, L., Structural changes in silicon anodes during lithium insertion/extraction. *Electrochemical and Solid State Letters* **2004**, *7* (5), A93.
- 2. Cao, P.-F.; Yang, G.; Li, B.; Zhang, Y.; Zhao, S.; Zhang, S.; Erwin, A.; Zhang, Z.; Sokolov, A. P.; Nanda, J., Rational design of a multifunctional binder for high-capacity silicon-based anodes. *ACS Energy Letters* **2019**, *4* (5), 1171-1180.
- 3. Schiele, A.; Breitung, B.; Hatsukade, T.; Berkes, B. z. B.; Hartmann, P.; Janek, J. r.; Brezesinski, T., The critical role of fluoroethylene carbonate in the gassing of silicon anodes for lithium-ion batteries. *ACS energy letters* **2017**, *2* (10), 2228-2233.
- 4. Qian, J.; Henderson, W. A.; Xu, W.; Bhattacharya, P.; Engelhard, M.; Borodin, O.; Zhang, J.-G., High rate and stable cycling of lithium metal anode. *Nature communications* **2015**, *6* (1), 1-9.
- 5. Goodenough, J. B.; Kim, Y., Challenges for rechargeable Li batteries. *Chemistry of materials* **2010**, 22 (3), 587-603.
- 6. Xu, K., Nonaqueous liquid electrolytes for lithium-based rechargeable batteries. *Chemical reviews* **2004**, *104* (10), 4303-4418.
- 7. Yin, Y.; Arca, E.; Wang, L.; Yang, G.; Schnabel, M.; Cao, L.; Xiao, C.; Zhou, H.; Liu, P.; Nanda, J., Nonpassivated Silicon Anode Surface. *ACS applied materials & interfaces* **2020**, *12* (23), 26593-26600.
- 8. Ashuri, M.; He, Q.; Shaw, L. L., Silicon as a potential anode material for Li-ion batteries: where size, geometry and structure matter. *Nanoscale* **2016**, *8* (1), 74-103.

- 9. Wang, A.; Kadam, S.; Li, H.; Shi, S.; Qi, Y., Review on modeling of the anode solid electrolyte interphase (SEI) for lithium-ion batteries. *npj Computational Materials* **2018**, *4* (1), 1-26.
- 10. An, S. J.; Li, J.; Daniel, C.; Mohanty, D.; Nagpure, S.; Wood III, D. L., The state of understanding of the lithium-ion-battery graphite solid electrolyte interphase (SEI) and its relationship to formation cycling. *Carbon* **2016**, *105*, 52-76.
- 11. Xu, C.; Lindgren, F.; Philippe, B.; Gorgoi, M.; Björefors, F.; Edström, K.; Gustafsson, T. r., Improved performance of the silicon anode for Li-ion batteries: understanding the surface modification mechanism of fluoroethylene carbonate as an effective electrolyte additive. *Chemistry of Materials* **2015**, 27 (7), 2591-2599.
- 12. Choi, N.-S.; Yew, K. H.; Lee, K. Y.; Sung, M.; Kim, H.; Kim, S.-S., Effect of fluoroethylene carbonate additive on interfacial properties of silicon thin-film electrode. *Journal of Power Sources* **2006**, *161* (2), 1254-1259.
- 13. Jin, Y.; Kneusels, N.-J. H.; Magusin, P. C.; Kim, G.; Castillo-Martínez, E.; Marbella, L. E.; Kerber, R. N.; Howe, D. J.; Paul, S.; Liu, T., Identifying the structural basis for the increased stability of the solid electrolyte interphase formed on silicon with the additive fluoroethylene carbonate. *Journal of the American Chemical Society* **2017**, *139* (42), 14992-15004.
- 14. Soto, F. A.; Ma, Y.; Martinez de la Hoz, J. M.; Seminario, J. M.; Balbuena, P. B., Formation and growth mechanisms of solid-electrolyte interphase layers in rechargeable batteries. *Chemistry of Materials* **2015**, *27* (23), 7990-8000.
- 15. Park, M. S.; Ma, S. B.; Lee, D. J.; Im, D.; Doo, S.-G.; Yamamoto, O., A highly reversible lithium metal anode. *Scientific reports* **2014**, *4*, 3815.
- 16. Ren, X.; Chen, S.; Lee, H.; Mei, D.; Engelhard, M. H.; Burton, S. D.; Zhao, W.; Zheng, J.; Li, Q.; Ding, M. S., Localized high-concentration sulfone electrolytes for high-efficiency lithium-metal batteries. *Chem* **2018**, *4* (8), 1877-1892.
- 17. Jaumann, T.; Balach, J.; Klose, M.; Oswald, S.; Eckert, J.; Giebeler, L., Role of 1, 3-dioxolane and LiNO3 addition on the long term stability of nanostructured silicon/carbon anodes for rechargeable lithium batteries. *Journal of The Electrochemical Society* **2016**, *163* (3), A557-A564.
- 18. Piwko, M.; Thieme, S.; Weller, C.; Althues, H.; Kaskel, S., Enabling electrolyte compositions for columnar silicon anodes in high energy secondary batteries. *Journal of Power Sources* **2017**, *362*, 349-357.
- 19. Etacheri, V.; Geiger, U.; Gofer, Y.; Roberts, G. A.; Stefan, I. C.; Fasching, R.; Aurbach, D., Exceptional electrochemical performance of Si-nanowires in 1, 3-dioxolane solutions: a surface chemical investigation. *Langmuir* **2012**, *28* (14), 6175-6184.
- 20. Ren, X.; Zou, L.; Cao, X.; Engelhard, M. H.; Liu, W.; Burton, S. D.; Lee, H.; Niu, C.; Matthews, B. E.; Zhu, Z., Enabling high-voltage lithium-metal batteries under practical conditions. *Joule* **2019**, *3* (7), 1662-1676.
- 21. Fong, R.; Von Sacken, U.; Dahn, J. R., Studies of lithium intercalation into carbons using nonaqueous electrochemical cells. *Journal of The Electrochemical Society* **1990**, *137* (7), 2009.
- 22. Jin, Y.; Kneusels, N.-J. H.; Marbella, L. E.; Castillo-Martínez, E.; Magusin, P. C.; Weatherup, R. S.; Jónsson, E.; Liu, T.; Paul, S.; Grey, C. P., Understanding fluoroethylene carbonate and vinylene carbonate based electrolytes for Si anodes in lithium ion batteries with NMR spectroscopy. *Journal of the American Chemical Society* **2018**, *140* (31), 9854-9867.
- 23. Hou, T.; Yang, G.; Rajput, N. N.; Self, J.; Park, S.-W.; Nanda, J.; Persson, K. A., The influence of FEC on the solvation structure and reduction reaction of LiPF6/EC electrolytes and its implication for solid electrolyte interphase formation. *Nano Energy* **2019**, *64*, 103881.
- 24. Li, J.; Dozier, A. K.; Li, Y.; Yang, F.; Cheng, Y.-T., Crack pattern formation in thin film lithiumion battery electrodes. *Journal of The Electrochemical Society* **2011**, *158* (6), A689.
- 25. Jung, H.; Park, M.; Yoon, Y.-G.; Kim, G.-B.; Joo, S.-K., Amorphous silicon anode for lithium-ion rechargeable batteries. *Journal of power sources* **2003**, *115* (2), 346-351.

- 26. Wu, Q.; Shi, B.; Bareño, J.; Liu, Y.; Maroni, V. A.; Zhai, D.; Dees, D. W.; Lu, W., Investigations of Si thin films as anode of lithium-ion batteries. *ACS applied materials & interfaces* **2018**, *10* (4), 3487-3494.
- 27. Yang, G.; Li, X.; Cheng, Y.; Wang, M.; Ma, D.; Sokolov, A. P.; Kalinin, S. V.; Veith, G. M.; Nanda, J., Distilling nanoscale heterogeneity of amorphous silicon using tip-enhanced Raman spectroscopy (TERS) via multiresolution manifold learning. *Nature communications* **2021**, *12* (1), 1-11.
- 28. Shen, B.; Wang, S.; Tenhaeff, W., Ultrathin conformal polycyclosiloxane films to improve silicon cycling stability. *Science advances* **2019**, *5* (7), eaaw4856.
- 29. Li, J.; Dudney, N. J.; Nanda, J.; Liang, C., Artificial solid electrolyte interphase to address the electrochemical degradation of silicon electrodes. *ACS applied materials & interfaces* **2014**, *6* (13), 10083-10088.
- 30. Yoon, T.; Chapman, N.; Seo, D. M.; Lucht, B. L., Lithium salt effects on silicon electrode performance and solid electrolyte interphase (SEI) structure, role of solution structure on SEI formation. *Journal of The Electrochemical Society* **2017**, *164* (9), A2082-A2088.
- 31. Stetson, C.; Yoon, T.; Coyle, J.; Nemeth, W.; Young, M.; Norman, A.; Pylypenko, S.; Ban, C.; Jiang, C.-S.; Al-Jassim, M., Three-dimensional electronic resistivity mapping of solid electrolyte interphase on Si anode materials. *Nano Energy* **2019**, *55*, 477-485.
- 32. Lee, J. G.; Kim, J.; Lee, J. B.; Park, H.; Kim, H.-S.; Ryu, J. H.; Jung, D. S.; Kim, E. K.; Oh, S. M., Mechanical damage of surface films and failure of nano-sized silicon electrodes in lithium ion batteries. *Journal of The Electrochemical Society* **2017**, *164* (1), A6103-A6109.
- 33. Yoon, T.; Xiao, C.; Liu, J.; Wang, Y.; Son, S.; Burrell, A.; Ban, C., Electrochemically induced fractures in crystalline silicon anodes. *Journal of Power Sources* **2019**, *425*, 44-49.
- 34. Swamy, T.; Chiang, Y.-M., Electrochemical charge transfer reaction kinetics at the silicon-liquid electrolyte interface. *Journal of The Electrochemical Society* **2015**, *162* (13), A7129-A7134.
- 35. Yang, J.; Liu, H.; Martens, W. N.; Frost, R. L., Synthesis and characterization of cobalt hydroxide, cobalt oxyhydroxide, and cobalt oxide nanodiscs. *The Journal of Physical Chemistry C* **2010**, *114* (1), 111-119.
- 36. Becker, D.; Cherkashinin, G.; Hausbrand, R.; Jaegermann, W., XPS study of diethyl carbonate adsorption on LiCoO2 thin films. *Solid State Ionics* **2013**, *230*, 83-85.
- 37. Schulz, N.; Hausbrand, R.; Dimesso, L.; Jaegermann, W., XPS-surface analysis of SEI layers on Li-ion cathodes: Part I. Investigation of initial surface chemistry. *Journal of The Electrochemical Society* **2018**, *165* (5), A819.
- 38. Guo, K.; Kumar, R.; Xiao, X.; Sheldon, B. W.; Gao, H., Failure progression in the solid electrolyte interphase (SEI) on silicon electrodes. *Nano Energy* **2020**, *68*, 104257.
- 39. Tokranov, A.; Kumar, R.; Li, C.; Minne, S.; Xiao, X.; Sheldon, B. W., Control and optimization of the electrochemical and mechanical properties of the solid electrolyte interphase on silicon electrodes in lithium ion batteries. *Advanced Energy Materials* **2016**, *6* (8), 1502302.
- 40. Schulz, N.; Hausbrand, R.; Wittich, C.; Dimesso, L.; Jaegermann, W., XPS-surface analysis of SEI layers on Li-ion cathodes: Part II. SEI-composition and formation inside composite electrodes. *Journal of The Electrochemical Society* **2018**, *165* (5), A833.
- 41. Camacho-Forero, L. E.; Balbuena, P. B., Elucidating electrolyte decomposition under electronrich environments at the lithium-metal anode. *Physical Chemistry Chemical Physics* **2017**, *19* (45), 30861-30873.
- 42. Lehmann, M. L.; Yang, G.; Gilmer, D.; Han, K. S.; Self, E. C.; Ruther, R. E.; Ge, S.; Li, B.; Murugesan, V.; Sokolov, A. P., Tailored crosslinking of Poly (ethylene oxide) enables mechanical robustness and improved sodium-ion conductivity. *Energy Storage Materials* **2019**, *21*, 85-96.
- 43. Michan, A. L.; Parimalam, B. S.; Leskes, M.; Kerber, R. N.; Yoon, T.; Grey, C. P.; Lucht, B. L., Fluoroethylene carbonate and vinylene carbonate reduction: Understanding lithium-ion battery electrolyte additives and solid electrolyte interphase formation. *Chemistry of Materials* **2016**, *28* (22), 8149-8159.

- 44. He, M.; Guo, R.; Hobold, G. M.; Gao, H.; Gallant, B. M., The intrinsic behavior of lithium fluoride in solid electrolyte interphases on lithium. *Proceedings of the National Academy of Sciences* **2020,** *117* (1), 73-79.
- 45. Han, S.-D.; Wood, K. N.; Stetson, C.; Norman, A. G.; Brumbach, M. T.; Coyle, J.; Xu, Y.; Harvey, S. P.; Teeter, G.; Zakutayev, A., Intrinsic Properties of Individual Inorganic Silicon–Electrolyte Interphase Constituents. *ACS applied materials & interfaces* **2019**, *11* (50), 46993-47002.
- 46. Lin, Y.-X.; Liu, Z.; Leung, K.; Chen, L.-Q.; Lu, P.; Qi, Y., Connecting the irreversible capacity loss in Li-ion batteries with the electronic insulating properties of solid electrolyte interphase (SEI) components. *Journal of Power Sources* **2016**, *309*, 221-230.
- 47. Camacho-Forero, L. E.; Smith, T. W.; Balbuena, P. B., Effects of high and low salt concentration in electrolytes at lithium–metal anode surfaces. *The Journal of Physical Chemistry C* **2017**, *121* (1), 182-194.
- 48. Bhatt, M. D.; O'Dwyer, C., The role of carbonate and sulfite additives in propylene carbonate-based electrolytes on the formation of SEI layers at graphitic Li-ion battery anodes. *Journal of the Electrochemical Society* **2014**, *161* (9), A1415.
- 49. Chew, H. B.; Hou, B.; Wang, X.; Xia, S., Cracking mechanisms in lithiated silicon thin film electrodes. *International Journal of Solids and Structures* **2014**, *51* (23-24), 4176-4187.
- 50. Cheng, Y.-T.; Verbrugge, M. W., Diffusion-induced stress, interfacial charge transfer, and criteria for avoiding crack initiation of electrode particles. *Journal of the Electrochemical Society* **2010**, *157* (4), A508.
- 51. Shin, H.; Park, J.; Han, S.; Sastry, A. M.; Lu, W., Component-/structure-dependent elasticity of solid electrolyte interphase layer in Li-ion batteries: experimental and computational studies. *Journal of Power Sources* **2015**, *277*, 169-179.
- 52. Jiao, S.; Ren, X.; Cao, R.; Engelhard, M. H.; Liu, Y.; Hu, D.; Mei, D.; Zheng, J.; Zhao, W.; Li, Q., Stable cycling of high-voltage lithium metal batteries in ether electrolytes. *Nature Energy* **2018**, *3* (9), 739-746.